

Tracking electrochemical reactions inside organic electrodes by *operando* IR spectroscopy



Jan Bitenc^{a,*}, Alen Vizintin^{a,1}, Jože Grdadolnik^a, Robert Dominko^{a,b,c}

^a National Institute of Chemistry, Hajdrihova 19, 1000, Ljubljana, Slovenia

^b Faculty of Chemistry and Chemical Technology, University of Ljubljana, Večna pot 113, 1000, Ljubljana, Slovenia

^c ALISTORE – European Research Institute, 33 rue Saint-Leu, Amiens, 80039, France

ABSTRACT

IR spectroscopy can be a non-destructive and straightforward probing tool in the battery research. However, its application has been limited due to the difficulties related to the handling and interpretation of *ex situ* samples along with the lack of widely applicable *in situ* and *operando* cells. Herein, we show a simple, *operando* ATR-IR two electrode pouch cell with an IR-transmissive silicon window and discuss its advantages and limitations. This setup is applied to the study of the poly-anthraquinone (PAQ) reaction mechanism in Li- and Mg-organic batteries. During the reduction/oxidation process of the PAQ, not only the conversion of both C=O groups into C-O⁻ species is observed, but also the formation of an intermediate semiquinone radical anion as an intermediate product. Furthermore, continuous measurement of IR spectra allows visualization of the gradual solid-electrolyte interphase (SEI) buildup on the cathode during cycling.

1. Introduction

To speed up the development of novel battery technologies (Li-rich, Na-ion, metal (Li, Ca, Mg, Al)-organic, metal-sulfur, metal-air batteries) [1–5], we need to develop new and improve current battery characterization techniques. An ideal battery characterization would be straightforward, non-invasive, non-destructive and optimized to probe specific battery chemistry. It should provide information about the electrochemical mechanism, degradation of the electrodes and electrolyte during prolonged cycling and allow real-time (*operando*) monitoring of the battery state-of-health. Ultimately, the developed *operando* techniques should enable real-time monitoring of the batteries and real-time detection of the battery degradation in their nascent state. This will be a major step towards the battery life extension and possible application of self-healing functionalities within the batteries [6].

In order to gain the information about the battery reaction mechanism, different spectroscopic techniques have already been applied, among others X-ray diffraction (XRD), X-ray absorption (XAS), nuclear magnetic resonance (NMR), transmission and scanning electron microscopy (TEM and SEM), Raman spectroscopy, ultraviolet–visible (UV–Vis) and IR spectroscopy [7–11]. One of the distinct advantages of IR spectroscopy is that the instruments are relatively inexpensive and broadly available. However, IR spectroscopy is underutilized in the battery research due to several reasons. Interpretation of data obtained from *ex*

situ samples can be quite complicated, because certain changes appear as weak and unspecific IR signals. Decomposition of *ex situ* samples in ambient or even under inert atmosphere complicates sample transfer and handling. Additionally, if not performed carefully, removal of the excess electrolyte from the cycled electrodes can be quite strenuous and cause degradation of the samples [12].

A solution to avoid these issues is use of electrochemical cells that enable *in situ* or even *operando* measurements. *Operando* measurements have a specific benefit of a continuous measurement of the IR spectra during the battery operation. In contrast with *ex situ* and *in situ*, the *operando* visualizes also transitional changes that can be overlooked during *ex situ* or *in situ* investigation. Typically, such setups require specially constructed electrochemical cells that minimize IR absorption by the bulk electrolyte and maximize the signal coming from the working electrode/electrolyte interface. Most often this is achieved by designing beaker cells, where working electrode is separated from the IR light guiding elements by a thin layer of electrolyte [13,14]. Another option is to coat the ATR crystals of the IR spectrometers directly with working electrodes and design electrochemical cells around them [15–17]. However, usage of beaker cells can affect the electrode/electrolyte ratio by significantly increasing the electrolyte amount for several times which introduces transport limitations between a thin working electrode/electrolyte layer and the bulk electrolyte. Design of new cells incorporating ATR crystals can be both time-consuming and costly, which

* Corresponding author.

E-mail address: jan.bitenc@ki.si (J. Bitenc).

¹ These authors contributed equally to this work.

makes their use interesting only for groups specialized in IR spectroscopy. Nevertheless, IR spectroscopy has demonstrated to be a straightforward, non-invasive, non-destructive and a universal technique to examine different battery chemistries [9,17–19], formation of a SEI [20] and electrolytes dynamics [16] during battery operation. IR spectroscopy examines the vibrational energy levels of molecular structure. Thus, it is very sensitive to the changes within the molecules involved in electrochemical process. The pioneering IR investigation of electrode/electrolyte interface was performed in the early eighties by Bewick and Pons [21,22]. Nowadays, the IR spectroscopy is found to be a useful characterization tool to probe different battery chemistries among post Li-ion batteries [9,17,18,20]. Recently, an improved method to probe the electrochemical mechanism of the organic cathodes within the metal-organic batteries was developed based on a new *operando* ATR-IR cell with Si wafer window, which allows measurements of the IR spectra during battery operation [9].

Herein we show a step forward in the *operando* ATR-IR application through measurements on polyanthraquinone cathode (PAQ) in Li- and Mg-organic battery. During the reduction/oxidation process of PAQ not only the transformation of both C=O groups into C–O[−] occurs, but also intermediate semiquinone radical anion is identified. Additionally, we discuss also limitations of the setup connected with the probing of the cathode backside, which are demonstrated through the study of the anthraquinone (AQ), which is a small and soluble organic molecule. During prolonged cycling formation of an SEI on the cathode surface is also visualized.

2. Material and methods

2.1. Synthesis

Anthraquinone (AQ) (99%) was purchased from commercial source (Fluka) and used without further purification. Polyanthraquinone (PAQ) was synthesized from the 1,4-dibromoanthraquinone monomer through cross-coupling polymerization [23]. The prepared polymer was purified by precipitation from chloroform (CHCl₃). Afterwards, short-chain oligomers were removed from the product during Soxhlet extraction in methanol. Final yield of the synthesis was 84%. More details about the synthesis can be found in SI.

2.2. Electrochemical characterization

The cathode composite was prepared by mixing active materials, Printex XE2 (Degussa) carbon black and PTFE binder in a mass ratio of 60:30:10. The self-standing composite was pressed on a carbon-coated Al mesh at 500 MPa. The Li cells were assembled in a spectro-electrochemical *operando* ATR-IR cell with a Li metal foil (FMC, thickness 500 μm) anode, Whatman GF/A glass fiber separator and 1 M LiTFSI (TFSI-bis(trifluoromethane)sulfonimide) in dimethoxyethane:1,3-dioxolane (DME:DOL) (1:1 vol %) as electrolyte. The cell was cycled in a potential window from 1.5 to 3 V vs Li/Li⁺ for Li-PAQ and from 1.5 to 3.5 V vs Li/Li⁺ for Li-AQ with a current density of 50 mA g^{−1} (C/5 rate). For the Mg-PAQ cell, Mg metal foil (Gallium Source, 99.95%, 50 μm) anode, Whatman GF/A glass fiber separator and 0.4 M Mg(TFSI)₂ 0.4 M MgCl₂ in tetraglyme: 1,3-dioxolane (TEG:DOL) (1:1 vol %) as electrolyte were used. The spectro-electrochemical cell was cycled in a potential window from 0.5 to 2.5 V vs Mg/Mg²⁺ with a current density of 50 mA g^{−1} (C/5 rate). The galvanostatic intermittent titration technique (GITT) was conducted on Li-AQ and Li-PAQ at C/5 current density in a potential window from 1.5 to 3.5 V and 1.5 to 3 V vs Li/Li⁺, respectively. The current was stopped every 20 min and the cell was left at open-circuit voltage (OCV) to relax until dE/dt reached less than 10 mV h^{−1}.

2.3. IR characterization

The spectro-electrochemical *operando* ATR-IR cell was prepared in a

two electrode pouch cell with a Si wafer (El-Cat Inc., 500 μm thickness, polished on both sides) [9]. The ATR-IR measurements were done on Bruker Vertex 80 equipped with a Specac Silver Gate Ge crystal ATR and a liquid nitrogen cooled mercury cadmium telluride (MCT) detector. The spectra were collected in absorbance mode with 64 scans at a resolution of 4 cm^{−1} in the range from 4000 to 500 cm^{−1}. The IR spectra were collected in *operando* mode with a series of repetitive scans every 2 min during galvanostatic cycling of the batteries with a current density of 50 mA g^{−1} (C/5 rate). The atmospheric compensation was performed on the IR spectra in OPUS version 7.8 software. The ATR difference spectra were obtained by subtracting the initial spectrum before the start of the electrochemical characterization from the obtained IR spectrum at a specific point of the discharge/charge.

2.4. Energy dispersive X-ray spectroscopy of *ex situ* cathodes

Three electrodes were examined, one soaked in Mg electrolyte overnight and two cycled electrodes. Among cycled electrodes, one was discharged to 0.5 V vs Mg/Mg²⁺, while the other one was recharged back to 2.5 V vs Mg/Mg²⁺. Afterwards, cells were taken back to the glove-box, where they were disassembled under inert atmosphere. All the electrodes were washed two times in 3 ml of dimethoxyethane (DME) for 10 min. Then they were dried for 2 h on vacuum at room temperature and transferred into scanning electron microscope with a vacuum transfer chamber to prevent exposure to the air atmosphere. Energy dispersive X-ray spectroscopy was performed on field emission SEM Carl Zeiss Supra VP 35 at 20 kV accelerating voltage.

3. Results and discussion

3.1. Spectro-electrochemical *operando* ATR-IR cell

The developed ATR-IR Si wafer pouch cell, where Si wafer window is inserted in the pouch cell foil on the working electrode side (Fig. 1) [9, 24], has several benefits over conventional spectro-electrochemical cells. The cell is basically the same as a typical lab pouch cell, which removes concerns connected with transport limitations from the beaker cells. Moreover, it can operate at low or even lean electrolyte conditions. Si wafer is relatively robust and can be easily sealed on the cell with the use of the thermo-bond film. The pouch cell also allows use of different current collectors. This becomes important for investigation of post-Li batteries, where in certain cases electrolytes are corrosive and non-compatible with typical current collectors (Al, Cu, stainless steel, Ni) [25]. Pouch cells can be easily manufactured with corrosion resistant metals like Pt, Au, Mo or W. Excellent sealing of the pouch cells enables measurements in the ambient atmosphere for several days or even weeks and removes the need for placing IR spectrometer inside the glove box (Fig. S1).

One of the limitations of this Si wafer pouch cell is that IR spectra contain additional signals coming from the thin layer of SiO₂ present on the Si wafer surface with intense bands at 1107 cm^{−1} due to Si–O–Si antisymmetric stretching vibration and Si–O–Si bending vibration at 615 cm^{−1} (Fig. S2). The intensities of the bands are between 0.1 and 0.2 absorbance unities for 1107 cm^{−1} and 0.2 and 0.3 absorbance unities for 615 cm^{−1}. This corresponds to approximately 80–60% and 60–50% of transmitted light. However, these bands can be effectively removed through subtraction procedure together with other electrochemically inactive bands (binder, electrolyte), which visualizes only IR bands that undergo changes during battery operation [9,24]. Another, more severe limitation is the fact that the electrode is being probed from the backside, i.e. electrode side opposite to the separator. This is not an issue in the case of sufficient IR penetration depth into the electrode or if the electrochemical performance of the electrode is homogenous along the whole thickness. However, in the case of soluble active materials, this can introduce certain artefacts. Thus, we decided to investigate the electrochemical mechanism of AQ cathode, which is a small, soluble molecule,

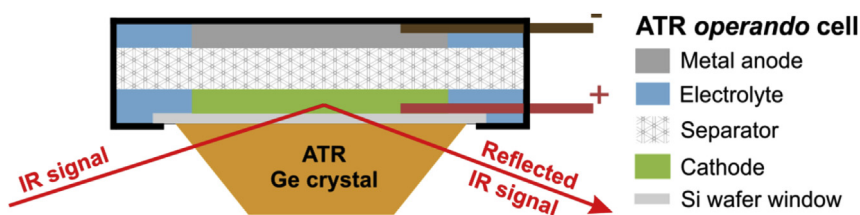


Fig. 1. Schematic representation of ATR-IR pouch cell on Ge ATR crystal.

in Li-AQ battery and also to determine IR penetration depth theoretically (SI).

Operando ATR-IR of AQ cathode showed surprising results (Fig. 2). IR spectra remained almost the same through the whole discharge plateau and the changes in difference IR spectra appeared only towards the end of the discharge. Even then, changes occurred in highly incremental way with the biggest changes at the end of the cycle. However, the changes still confirm the reduction of carbonyl bond at 1672 cm^{-1} and appearance of new -C-O^- band at 1378 cm^{-1} upon discharge, which shows good agreement with literature reports [9,26]. Behavior in the charge was similar with most intense changes at the start of the cycle and increasingly smaller changes in the second half of the charge. At the end of charge small decrease of carbonyl band could still be detected, most likely as a consequence of a local decrease in AQ concentration due to dissolution. We can conclude that the observed IR active changes still correspond to the actual electrochemical mechanism. However, the measured IR spectra at the backside of the cathode are not representative for the whole cathode and cannot be time correlated with electrochemical cycling. Such behavior is caused by dissolution of AQ, which causes inhomogeneity in electrode performance along its thickness and limited penetration depth of our ATR-IR setup. To verify results of constant current experiment, we performed characterization of AQ cathode in galvanostatic intermittent titration technique (GITT), which revealed similar behavior, only changes of IR bands occurred a bit sooner during specific cycle step (Figs. S3 and S4).

Probed thickness (d_p) of our electrode is defined by the penetration of

the evanescent wave. This is, in general, determined by the wavelength of the light (λ), angle of incidence (θ) and refraction indices of the Si wafer (n_1) and the probed medium (n_2) according to equation (1) (for details see SI).

$$d_p = \frac{\lambda}{2\pi\sqrt{n_1^2 \sin^2 \theta - n_2^2}} \quad (1)$$

High refractive index of Si ($n_1 = 3.42$) means that penetration depth is relatively low and is somewhere in the range from 0.16 to $1.06\ \mu\text{m}$ (detailed calculation can be found in the SI). Estimated thickness of our electrodes was up to $150\ \mu\text{m}$ (Fig. S5), which means that we probed only a small part of the electrode. In the case of insoluble polymers, where cathode active material does not dissolve, this is not a problem, but in the case of soluble AQ cathode it leads to significantly delayed IR spectral response. This limitation should be taken into account, especially when dealing with soluble active materials.

3.2. Electrochemical performance and *operando* ATR-IR analysis of Li- and Mg-PAQ battery

To demonstrate the straightforward application of the *operando* ATR-IR spectroscopy to non-soluble active materials, we have investigated the polyanthraquinone (PAQ) performance in Li- and Mg-organic battery. PAQ is an anthraquinone (AQ) family polymer prepared by a cross-coupling polymerization. It exhibits both good capacity retention and rate capability in both Mg and Li batteries [27,28]. However, maximum

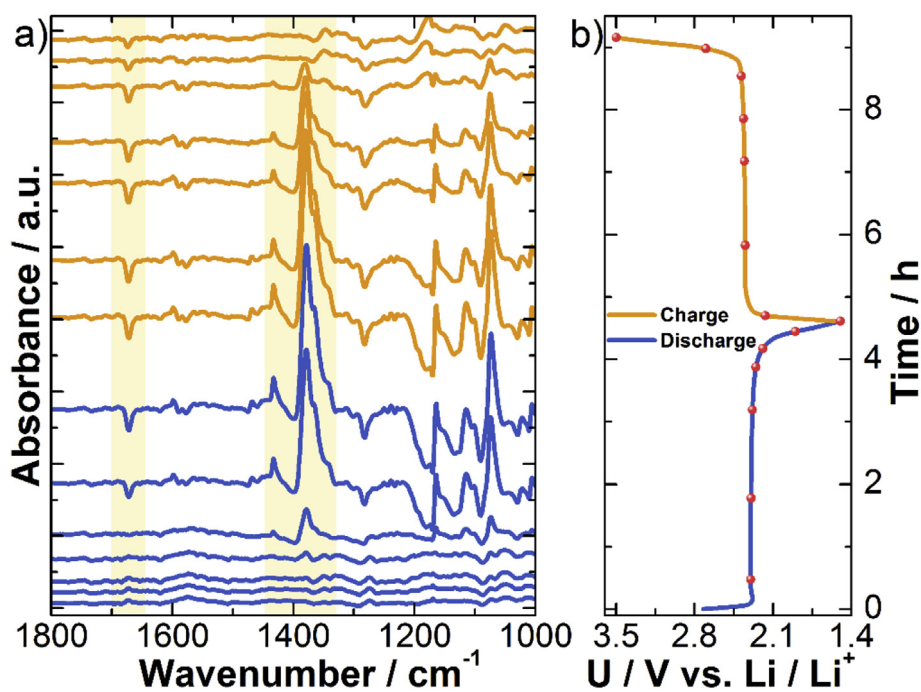


Fig. 2. *Operando* ATR-IR characterization of Li-AQ battery during first cycle. a) Difference spectra of AQ cathode during first cycle in Li battery. b) Corresponding galvanostatic cycle of AQ cathode at the C/5 current density in 1 M LiTFSI DOL:DME (1:1 vol%). Red circle marks in the galvanostatic curve correspond to the measurement points of IR spectra. (For interpretation of the references to colour in this figure legend, the reader is referred to the Web version of this article.)

practical capacities in Li and Mg electrolytes are significantly different. Maximum practical capacity in Li battery is close to the theoretical value (260 mAh g^{-1}) [27], while the maximum capacity in Mg is considerably lower, only slightly above 50% of the theoretical one (133 mAh g^{-1}) [28]. This suggests that the electrochemical mechanism might change from Li to Mg battery or that the performance of PAQ is worse in Mg electrolyte. Our electrochemical tests suggest that the difference between the two electrolytes is smaller. PAQ cathode could reach 219 mAh g^{-1} of capacity in the Li electrolyte and 148 mAh g^{-1} of the capacity in Mg electrolyte (Fig. 3). In both systems PAQ cathode exhibits a single voltage plateau at 2.1 V and 1.4 V in Li and Mg battery, respectively. In the first cycle the discharge capacity of Mg-PAQ battery is limited due to high polarization of the cell originating from Mg anode, which is a consequence of partial Mg anode passivation by a TFSI⁻ anion [29]. This polarization is especially pronounced during the start of the cycling and causes the discharge voltage to drop below 1.0 V at the start of the first discharge. Although, the polarization of Mg cell significantly decreases after the first cycle, it remained significantly larger compared to the Li-PAQ also in latter cycles.

While both systems exhibit a single slightly sloped voltage plateau, it is not clear if anthraquinone groups within the polymer undergo a one-step two electron or a two-step one electron reduction and if there is any difference between the two electrolytes. The *operando* investigation of Li-PAQ cathode polymer during cycling (Fig. 4) reveals not only decrease of carbonyl bond at 1668 cm^{-1} and appearance of new $\text{C-O}^- \text{Li}^+$ band at 1374 cm^{-1} like in previous reports [9,26], but also additional peaks at 1493 and 1397 cm^{-1} . These two bands start to appear immediately after the start of the discharge and have the highest intensity in the middle of both half cycles.

Bands observed at 1493 and 1397 cm^{-1} belong to the semiquinone radical anion [30], which is the intermediate product of PAQ reduction, after polymer accepts one electron per active AQ group (Scheme 1).

Presence of semiquinone radical anion bands has already been observed in the IR analysis of the AQ dissolved within the electrolyte in specially designed cell for a liquid IR characterization [30]. However, it was never confirmed in a practical battery setup, where due to the lack of *operando* techniques only *ex situ* results with limited resolution and reliability were investigated [26,31]. To inspect the nature of semiquinone radical anion we performed *operando* ATR-IR measurements under GITT mode (Figs. S6 and S7). GITT characterization revealed that semiquinone bands are stable under open circuit conditions. Hence, semiquinone radical anion is an equilibrium species. During discharge also $\text{C}=\text{C}$ stretching vibration at 1592 cm^{-1} decreases. Furthermore, changes in the ring vibrations including $\text{C}-\text{C}$ stretchings and in-plane $\text{C}-\text{H}$ bendings can be seen as a decrease of the intensity for vibrations at 1327 , 1308 , 1251 and 1117 cm^{-1} and increase of the intensity for vibrations at 1069 and 1047 cm^{-1} upon discharge. At the end of the first cycle we can also observe formation of the SEI layer on the cathode as low intensity IR peaks at 1350 , 1325 , 1182 , 1054 cm^{-1} that belong to the in and out of phase antisymmetric SO_2 stretchings, symmetric SO_2 and $\text{C}-\text{F}$ stretchings and antisymmetric $\text{S}-\text{N}-\text{S}$ stretching, respectively. These vibrations imply presence of TFSI⁻ anion or its constituent groups in the cathode SEI. These SEI peaks become even more apparent, when we subtract the spectrum before the start of the cycling from the spectrum at the start or the end of the 6th cycle (Fig. S8). The subtraction reveals increased intensity of these peaks and also significant inclination in the background below 1300 cm^{-1} [32,33].

The main question regarding the Mg-PAQ battery is if the divalent nature of a magnesium ion changes the reaction mechanism of the PAQ cathode. In the first cycle the discharge capacity is limited due to high polarization of the cell mentioned before, but the *operando* ATR-IR still visualizes identical IR spectra changes (Fig. S9) as in latter cycles (Fig. 5). However, the difference between obtained capacities in first (99 mAh g^{-1}) and third (132 mAh g^{-1}) discharge, increases intensity of IR changes during third cycle. Thus, we focus our analysis on the third cycle. *Operando* ATR-IR investigation in Mg electrolyte demonstrates that PAQ

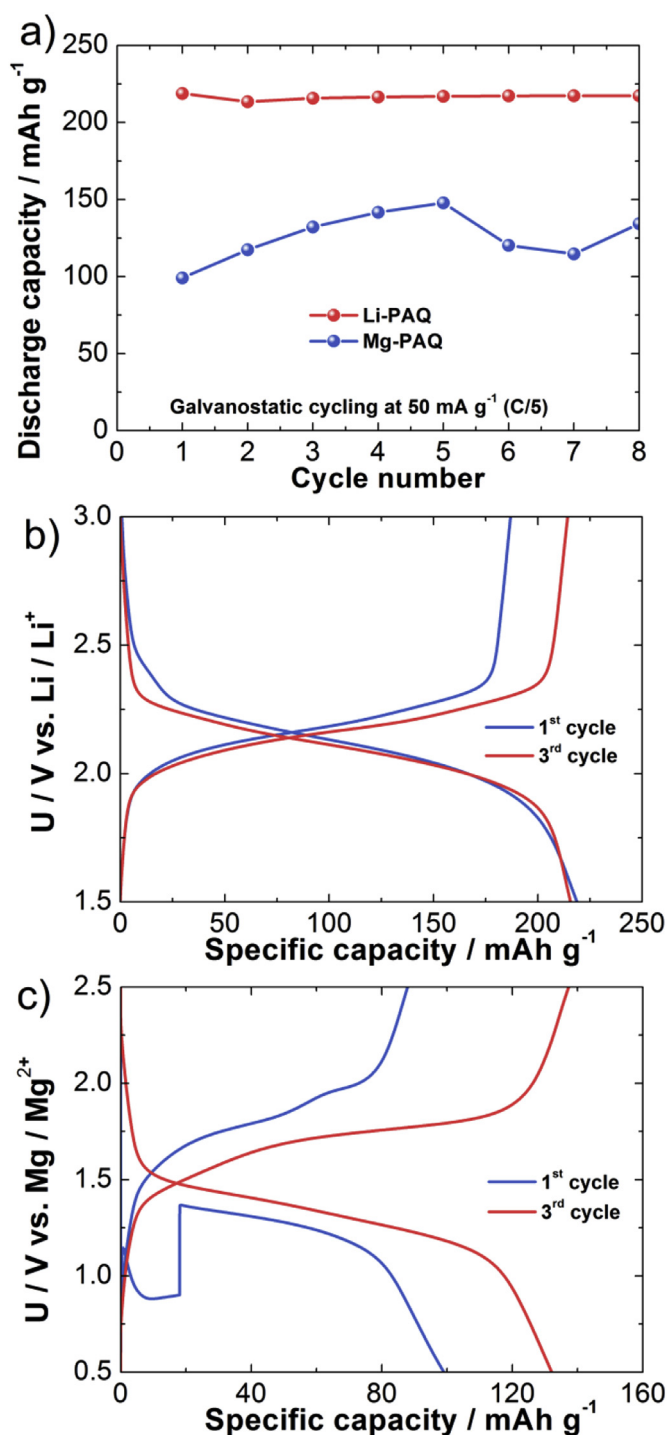


Fig. 3. a) Discharge capacity for PAQ in Li (red) and Mg (blue) battery at a current density of 50 mA g^{-1} (C/5), b) galvanostatic discharge/charge cycles for the Li-PAQ battery at a current density of 50 mA g^{-1} (C/5), and c) galvanostatic discharge/charge cycles for the Mg-PAQ battery at a current density of 50 mA g^{-1} (C/5). (For interpretation of the references to colour in this figure legend, the reader is referred to the Web version of this article.)

reduction proceeds through the same steps as in Li electrolyte. First, formation of the semiquinone radical anion and formation of the dianion at the end of discharge (Scheme 1).

There is a small shift of the IR bands for both semiquinone radical anion, which appears at 1483 and 1386 cm^{-1} , and the IR band of the final dianion, which is also slightly upshifted to 1376 cm^{-1} , compared with the ones from the Li analogue. Moreover, differences between the

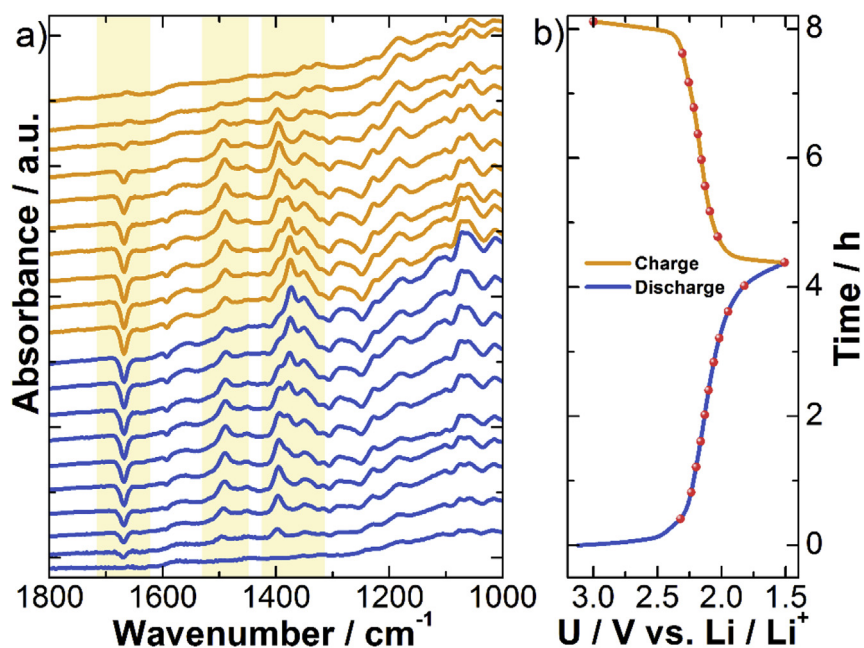
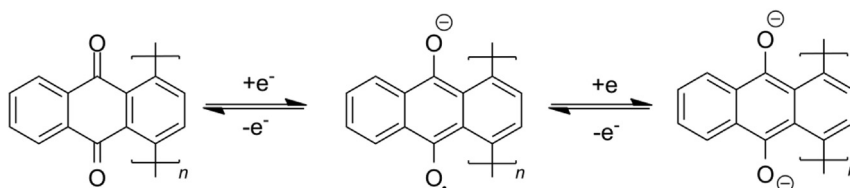


Fig. 4. *Operando* ATR-IR characterization of Li-PAQ battery during first cycle. a) Difference spectra of PAQ cathode during first cycle in Li battery. b) Corresponding galvanostatic cycle of PAQ cathode at the C/5 current density in 1 M LiTFSI DOL:DME (1:1 vol %). Red circle marks in the galvanostatic curve correspond to the measurement points of IR spectra. (For interpretation of the references to colour in this figure legend, the reader is referred to the Web version of this article.)



Scheme 1. Electrochemical mechanism of PAQ reduction proceeds as a two-step one electron reaction through formation of semi-quinone radical anion.

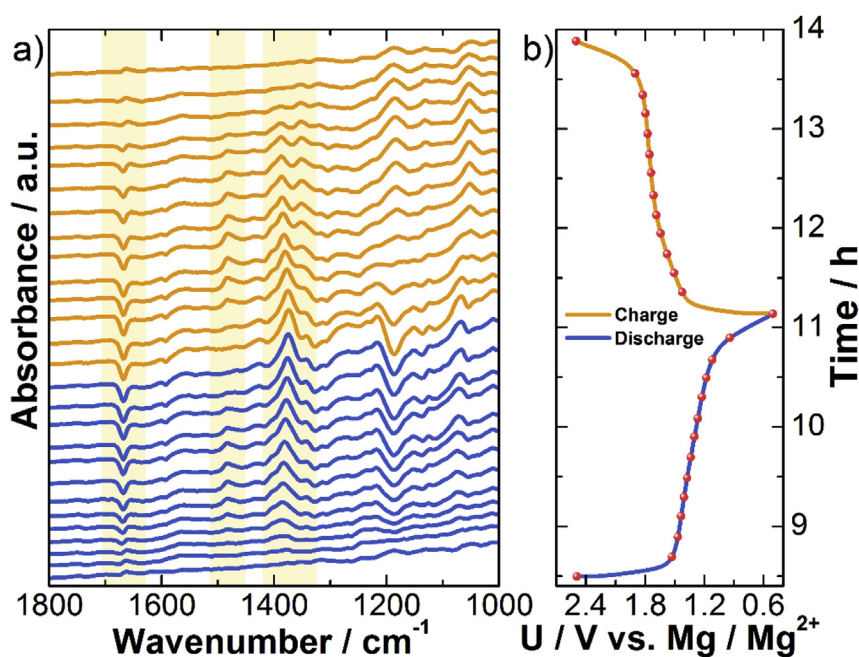


Fig. 5. *Operando* ATR-IR characterization of Mg-PAQ battery during third cycle. a) Difference spectra of PAQ cathode during third cycle in Mg battery. b) Corresponding galvanostatic cycle of PAQ cathode at the C/5 current density in 0.4 M Mg (TFSI)₂ 0.4 M MgCl₂ TEG:DOL (1:1 vol %). Red circle marks in the galvanostatic curve correspond to the measurement points of IR spectra. (For interpretation of the references to colour in this figure legend, the reader is referred to the Web version of this article.)

changes in Li and Mg batteries are visible in the finger print region of the IR spectra (Figs. 4 and 5), where ring vibrations of C–C stretching and in-plane C–H bending are present. In the Mg-PAQ battery a formation of a new reversible peak at 1188 cm^{-1} during the discharge and charge is observed. The ring vibration changes in the finger print suggest a conformational changes of the PAQ polymer due to the interaction with Mg^{2+} ions [9]. ATR-IR spectra demonstrate that reduction of PAQ in Mg electrolyte is complete and proceeds in two-step one electron reduction into PAQ dianion. Two-steps reaction means that the cation that serves as a counter ion for semiquinone radical anion is either monovalent or bivalent Mg cation that interacts with two single charge semiquinone radical anions. First hypothesis is in good agreement with the recent report, where it was shown that in the Mg-organic batteries tested in MgCl_2 containing electrolytes, MgCl^+ species can serve as counter ions [34]. MgCl^+ role as counter ion has a negative effect on the overall energy density of the battery since MgCl_2 containing electrolyte can become the capacity limiting factor. To confirm the exact electrochemical nature of the Mg counter ion involved in the reduction of PAQ we complemented our measurements with the EDS analysis of *ex situ* PAQ electrodes (Table S1). No Mg or Cl was detected on the electrode that was soaked in the Mg electrolyte overnight, while Mg and Cl could be detected in both discharged and charged Mg electrodes. However, the amount of both elements was around 10 times higher in the discharged than in charged electrode; residual Mg and Cl in charged electrode can be explained by the incomplete first charge of the PAQ cathode. The atomic ratio between the Mg and Cl is 2.5 and 2.9 in the discharged and charged electrode, respectively. The measured ratios mean that discharged PAQ is not coordinated exclusively with Mg^{2+} or MgCl^+ , but both at the same time. With approximately 75% of the reduced anthraquinone groups in the discharged PAQ being coordinated by Mg^{2+} and 25% of the groups coordinated by the MgCl^+ . This in fact means that Mg^{2+} cations most likely coordinate also semiquinone radical anions. Moreover, after the end of the first and especially third cycle, we can observe broad peaks of cathode SEI at 1316, 1183 and 1050 cm^{-1} and again inclination of the background below 1300 cm^{-1} , similar to the formation of SEI in Li battery (Fig. S8).

4. Conclusion

Use of the Si wafer window in the two electrode pouch cells enables simplified *operando* ATR-IR measurements in ambient conditions without the need to construct new and sophisticated ATR-IR battery cells. Furthermore, it enables measurement conditions (electrolyte amount, separators, current density) that are same as in laboratory pouch cell setup, which simplifies correlation between the electrochemical results obtained in lab cells and *operando* measurements. Limitations of this cell are connected with the probing of the electrode backside and demonstrated in the case of Li–AQ battery employing small AQ cathode material, soluble in electrolyte. A big time delay is observed between the electrochemical activity of AQ cathode and its ATR-IR spectra. Pouch cell with the IR-transmissive Si wafer window is further utilized for identification of electrochemical mechanism of PAQ in Li and Mg batteries, where for the first time presence of the intermediate semiquinone radical anion is detected during discharge in both battery systems. Presence of semiquinone radical anion in Mg electrolyte could support recent finding about MgCl^+ storage in Mg–organic batteries in MgCl_2 containing electrolytes. However, our EDS investigation of *ex situ* cathode reveals that while both MgCl^+ and Mg^{2+} storage are taking place in our Mg-PAQ battery, Mg^{2+} is the dominating species, which also interacts with the intermediate semiquinone radical anion. The presented method can be further elaborated to the study of the SEI formation and effect of the different additives as shown by detection of the gradual SEI build up on the cathodes during initial cycles. Being both powerful and simple characterization method for elucidation of electrochemical mechanism and degradation, we can anticipate that the *operando* ATR-IR pouch cell with a Si wafer window will find broad applicability in the battery community and beyond.

Acknowledgements

Authors thank Jernej Bobnar for his assistance with the SEM vacuum transfer chamber. Financial support from the Slovenian Research Agency (research project J2-8167, research core funding P2-0393) and Honda R&D Europe (Germany) is gratefully acknowledged and appreciated.

Appendix A. Supplementary data

Supplementary data to this article can be found online at <https://doi.org/10.1016/j.ensm.2019.05.038>.

References

- [1] D. Larcher, J.-M. Tarascon, Towards greener and more sustainable batteries for electrical energy storage, *Nat. Chem.* 7 (2015) 19–29, <https://doi.org/10.1038/nchem.2085>.
- [2] G. Assat, J.-M. Tarascon, Fundamental understanding and practical challenges of anionic redox activity in Li-ion batteries, *Nat. Energy* 3 (2018) 373–386, <https://doi.org/10.1038/s41560-018-0097-0>.
- [3] M. Armand, J.M. Tarascon, Building better batteries, *Nature* 451 (2008) 2–7.
- [4] D. Aurbach, Z. Lu, A. Schechter, Y. Gofer, H. Gizbar, R. Turgeman, Y. Cohen, M. Moshkovich, E. Levi, Prototype systems for rechargeable magnesium batteries, *Nature* 407 (2000) 724–727, <https://doi.org/10.1038/35037553>.
- [5] P. Canepa, G. Sai Gautam, D.C. Hannah, R. Malik, M. Liu, K.G. Gallagher, K.A. Persson, G. Ceder, Odyssey of multivalent cathode materials: open questions and future challenges, *Chem. Rev.* 117 (2017) 4287–4341, <https://doi.org/10.1021/acs.chemrev.6b00614>.
- [6] C.P. Grey, J.M. Tarascon, Sustainability and in situ monitoring in battery development, *Nat. Mater.* 16 (2016) 45–56, <https://doi.org/10.1038/nmat4777>.
- [7] A. Vizintin, L. Chabanne, E. Tchernychova, I. Arçon, L. Stievano, G. Aquilanti, M. Antonietti, T.-P. Feller, R. Dominko, The mechanism of Li_2S activation in lithium-sulfur batteries: can we avoid the polysulfide formation? *J. Power Sources* 344 (2017) 208–217, <https://doi.org/10.1016/j.jpowsour.2017.01.112>.
- [8] M.U.M. Patel, R. Demir-Cakan, M. Morcrette, J.-M. Tarascon, M. Gaberscek, R. Dominko, Li-S battery analyzed by UV/vis in *operando* mode, *ChemSusChem* 6 (2013) 1177–1181, <https://doi.org/10.1002/cssc.201300142>.
- [9] A. Vizintin, J. Bitenc, A. Kopač Lautar, K. Pirnat, A. Grdadolnik, J. Stare, A. Radon-Vitanova, R. Dominko, Probing electrochemical reactions in organic cathode materials via in *operando* infrared spectroscopy, *Nat. Commun.* 9 (2018) 661, <https://doi.org/10.1038/s41467-018-03114-1>.
- [10] J. Hannauer, J. Scheers, J. Fullenwarth, B. Fraisse, L. Stievano, P. Johansson, The quest for polysulfides in lithium-sulfur battery electrolytes: an *operando* confocal Raman spectroscopy study, *ChemPhysChem* 16 (2015) 2755–2759, <https://doi.org/10.1002/cphc.201500448>.
- [11] R. Bhattacharyya, B. Key, H. Chen, A.S. Best, A.F. Hollenkamp, C.P. Grey, In situ NMR observation of the formation of metallic lithium microstructures in lithium batteries, *Nat. Mater.* 9 (2010) 504–510, <https://doi.org/10.1038/nmat2764>.
- [12] K.V. Kravchik, S. Wang, L. Piveteau, M.V. Kovalenko, Efficient aluminum chloride-natural graphite battery, *Chem. Mater.* 29 (2017) 4484–4492, <https://doi.org/10.1021/acs.chemmater.7b01060>.
- [13] N.S. Marinković, M. Hecht, J.S. Loring, W.R. Fawcett, A sifnirs study of the diffuse double layer at single crystal platinum electrodes in acetonitrile, *Electrochim. Acta* 41 (1996) 641–651, [https://doi.org/10.1016/0013-4686\(95\)00352-5](https://doi.org/10.1016/0013-4686(95)00352-5).
- [14] E.V. Carino, J. Staszak-Jirkovsky, R.S. Assary, L.A. Curtiss, N.M. Markovic, F.R. Brushett, Tuning the stability of organic active materials for nonaqueous redox flow batteries via reversible, electrochemically mediated Li^+ coordination, *Chem. Mater.* 28 (2016) 2529–2539, <https://doi.org/10.1021/acs.chemmater.5b04053>.
- [15] H. Ataee-Esfahani, D.-J. Chen, Y.-J. Tong, Dual-IR window/electrode *operando* attenuated total reflection-IR absorption spectroscopy for battery research, *Batter. Supercaps.* (2018), <https://doi.org/10.1002/batt.201800068>.
- [16] C. Marino, A. Boulaoued, J. Fullenwarth, D. Maurin, N. Louvain, J.-L. Bantignies, L. Stievano, L. Monconduit, Solvation and dynamics of lithium ions in carbonate-based electrolytes during cycling followed by *operando* infrared spectroscopy: the example of NiSb_2 , a typical negative conversion-type electrode material for lithium batteries, *J. Phys. Chem. C* 121 (2017) 26598–26606, <https://doi.org/10.1021/acs.jpcc.7b06685>.
- [17] J.P. Vivek, N.G. Berry, J. Zou, R.J. Nichols, L.J. Hardwick, In situ surface-enhanced infrared spectroscopy to identify oxygen reduction products in nonaqueous metal–oxygen batteries, *J. Phys. Chem. C* 121 (2017) 19657–19667, <https://doi.org/10.1021/acs.jpcc.7b06391>.
- [18] N. Saqib, G.M. Ohlhausen, J.M. Porter, In *operando* infrared spectroscopy of lithium polysulfides using a novel spectro-electrochemical cell, *J. Power Sources* 364 (2017) 266–271, <https://doi.org/10.1016/j.jpowsour.2017.08.030>.
- [19] M. Matsui, S. Deguchi, H. Kuwata, N. Imanishi, In-*operando* FTIR spectroscopy for composite electrodes of lithium-ion batteries, *Electrochemistry* 83 (2015) 874–878, <https://doi.org/10.5796/electrochemistry.83.874>.
- [20] Y. Deng, S. Dong, Z. Li, H. Jiang, X. Zhang, X. Ji, Applications of conventional vibrational spectroscopic methods for batteries beyond Li-ion, *Small Methods* 2 (2018) 1700332, <https://doi.org/10.1002/smt.201700332>.

- [21] A. Bewick, K. Kunimatsu, B. Stanley Pons, Infra red spectroscopy of the electrode-electrolyte interphase, *Electrochim. Acta* 25 (1980) 465–468, [https://doi.org/10.1016/0013-4686\(80\)87039-3](https://doi.org/10.1016/0013-4686(80)87039-3).
- [22] S. Pons, The use of fourier transform infrared spectroscopy for in situ recording of species in the electrode-electrolyte solution interphase, *J. Electroanal. Chem. Interfacial Electrochem.* 150 (1983) 495–504, [https://doi.org/10.1016/S0022-0728\(83\)80229-0](https://doi.org/10.1016/S0022-0728(83)80229-0).
- [23] T. Yamamoto, T. Kimura, K. Shiraiishi, Preparation of π -conjugated polymers composed of hydroquinone, p-benzoquinone, and p-diacetoxyphenylene units. Optical and redox properties of the polymers, *Macromolecules* 32 (1999) 8886–8896, <https://doi.org/10.1021/ma9907946>.
- [24] T. Bančić, J. Bitenc, K. Pirnat, A. Kopač Lautar, J. Grdadolnik, A. Randon Vitanova, R. Dominko, Electrochemical performance and redox mechanism of naphthalene-hydrazine diimide polymer as a cathode in magnesium battery, *J. Power Sources* 395 (2018) 25–30, <https://doi.org/10.1016/j.jpowsour.2018.05.051>.
- [25] C. Wall, Z. Zhao-Karger, M. Fichtner, Corrosion resistance of current collector materials in bisamide based electrolyte for magnesium batteries, *ECS Electrochem. Lett.* 4 (2014), <https://doi.org/10.1149/2.0111501eel>. C8–C10.
- [26] B. Tian, G.-H. Ning, W. Tang, C. Peng, D. Yu, Z. Chen, Y. Xiao, C. Su, K.P. Loh, Polyquinoneimines for lithium storage: more than the sum of its parts, *Mater. Horiz.* 3 (2016) 429–433, <https://doi.org/10.1039/C6MH00072J>.
- [27] Z. Song, Y. Qian, M.L. Gordin, D. Tang, T. Xu, M. Otani, H. Zhan, H. Zhou, D. Wang, Polyanthraquinone as a reliable organic electrode for stable and fast lithium storage, *Angew. Chem. Int. Ed.* 54 (2015) 13947–13951, <https://doi.org/10.1002/anie.201506673>.
- [28] B. Pan, J. Huang, Z. Feng, L. Zeng, M. He, L. Zhang, J.T. Vaughey, M.J. Bedzyk, P. Fenter, Z. Zhang, A.K. Burrell, C. Liao, Polyanthraquinone-based organic cathode for high-performance rechargeable magnesium-ion batteries, *Adv. Energy Mater.* 6 (2016) 1600140, <https://doi.org/10.1002/aenm.201600140>.
- [29] O. Tutusaus, R. Mohtadi, N. Singh, T.S. Arthur, F. Mizuno, Study of electrochemical phenomena observed at the Mg metal/electrolyte interface, *ACS Energy Lett.* 2 (2017) 224–229, <https://doi.org/10.1021/acsenerylett.6b00549>.
- [30] M. Büschel, C. Stadler, C. Lambert, M. Beck, J. Daub, Heterocyclic quinones as core units for redox switches: UV-vis/NIR, FTIR spectroelectrochemistry and DFT calculations on the vibrational and electronic structure of the radical anions, *J. Electroanal. Chem.* 484 (2000) 24–32, [https://doi.org/10.1016/S0022-0728\(00\)00037-1](https://doi.org/10.1016/S0022-0728(00)00037-1).
- [31] W. Wan, H. Lee, X. Yu, C. Wang, K.-W. Nam, X.-Q. Yang, H. Zhou, Tuning the electrochemical performances of anthraquinone organic cathode materials for Li-ion batteries through the sulfonic sodium functional group, *RSC Adv.* 4 (2014) 19878–19882, <https://doi.org/10.1039/C4RA01166J>.
- [32] D. Aurbach, I. Weissman, A. Zaban, O. Chusid, Correlation between surface chemistry, morphology, cycling efficiency and interfacial properties of Li electrodes in solutions containing different Li salts, *Electrochim. Acta* 39 (1994) 51–71, [https://doi.org/10.1016/0013-4686\(94\)85010-0](https://doi.org/10.1016/0013-4686(94)85010-0).
- [33] O. Chusid, Y. Gofer, D. Aurbach, M. Watanabe, T. Momma, T. Osaka, Studies of the interface between lithium electrodes and polymeric electrolyte systems using in situ FTIR spectroscopy 98 (2001) 632–636.
- [34] H. Dong, Y. Liang, H. Dong, Y. Liang, O. Tutusaus, R. Mohtadi, Y. Zhang, F. Hao, Y. Yao, Directing Mg-storage chemistry in organic polymers toward high-energy Mg batteries directing Mg-storage chemistry in organic polymers toward high-energy Mg batteries, *Joule* (2019) 1–12, <https://doi.org/10.1016/j.joule.2018.11.022>.